
IEEE International AP-S Symposium
July 2008
Symposium Digest
IEEE
A P S
U.R.S.I.
San Diego
USNC/URSI National Radio Science Meeting

Chamber Imaging Using Spherical Near-Field Scanning

R. C. Wittmann, M. H. Francis, and R. H. Direen
National Institute of Standards and Technology, Boulder, CO 80305,
Email: francis@boulder.nist.gov

Introduction

We discuss recent measurements performed at the National Institute of Standards and Technology (NIST) that were used to characterize the incident fields within a test volume and to produce images of the test chamber. The probe (Figure 1), on a roll-over-azimuth mount, was scanned over a spherical surface enclosing the test volume. A ladder with a small metal plate (Figure 2) and a bicycle (Figure 1) were both included in the scene. Illumination was alternately provided by standard gain horns mounted on the wall and on a tripod (Figure 3) in the first measurement setup and a cassegrain dish mounted on the wall and a circular waveguide on a tripod in setup 2. In setup 1, we used a probe with a gain of about 7 dB, while in setup 2 we used a probe with a gain of about 22 dB.

The origin of the laboratory coordinate system is the center of the measurement sphere, the x axis is directed (horizontally) from this origin through the middle of the wall horn aperture, and the z axis is directed upward. Polar angles θ and φ are defined in the usual manner. When $\theta = 0°$ the probe points toward the ceiling; when $\theta = 90°$and $\varphi = 0°$, the probe points toward the wall horn; and when $\theta = 90°$and $\varphi = 90°$, the probe points in the y direction. This coordinate system is used in the collection, analysis, and presentation of the data.

Measurements were made at 16 GHz, the measurement sphere radius was $r_p = 64$ cm (in measurement 1) and $r_p = 75$ cm in measurement 2. The data were collected at 0.75° increments in θ and φ in measurement 1 and 0.6° increments in measurement 2.

Theory

The technique is based on a plane-wave representation of the incident field

$$\mathbf{E}_i(\mathbf{r}) \approx \frac{1}{4\pi} \int \mathbf{a}_N\left(\hat{\mathbf{k}}\right) \exp\left(i\mathbf{k}\cdot\mathbf{r}\right) d\hat{\mathbf{k}} \tag{1}$$

$$\mathbf{a}_N(\hat{\mathbf{r}}) = \sum_{n=1}^{N} \sum_{m=-n}^{n} \left[a_{nm}^1 \mathbf{X}_{nm}(\hat{\mathbf{r}}) + a_{nm}^2 \mathbf{Y}_{nm}(\hat{\mathbf{r}})\right], \tag{2}$$

where the integral is over 4π sr, $k = |\mathbf{k}| = 2\pi/\lambda$, and $\mathbf{X}_{nm}$ and $\mathbf{Y}_{nm}$ are vector spherical harmonics [1, chapter 16]. Here, $N \sim kr_p$.

978-1-4244-2042-1/08/$25.00 ©2008 IEEE

The algorithm described in [2] allows calculation of the coefficients a^1_{nm} and a^2_{nm} from the measured data. Once these coefficients are known, then (1) can be used to determine the field anywhere *inside the test volume.* The theory accounts for probe pattern effects; that is, we do not need to assume that the probe measures the electric field directly.

An image can be formed by simply plotting $|\mathbf{a}_N(\hat{\mathbf{r}})|$. For example, it is apparent from (1) that the image of the plane wave $\mathbf{E}_0 \exp(i\mathbf{k}_0 \cdot \mathbf{r})$ must be proportional to $\left|\delta_N\left(\hat{\mathbf{r}} - \hat{\mathbf{k}}_0\right)\right|$, where δ_N approaches the Dirac delta function as $N \to \infty$. The angular resolution (Rayleigh criterion) is inversely proportional to N [3]

$$\Delta\theta \approx \frac{3.83}{N}. \tag{3}$$

An image of a plane wave will also exhibit sidelobes extending away from the central peak. The sidelobe level can be reduced using window functions, resulting in the usual trade-off between resolution and dynamic range. Images may also be focused at finite distances, rather than at infinity. For details, please see [3].

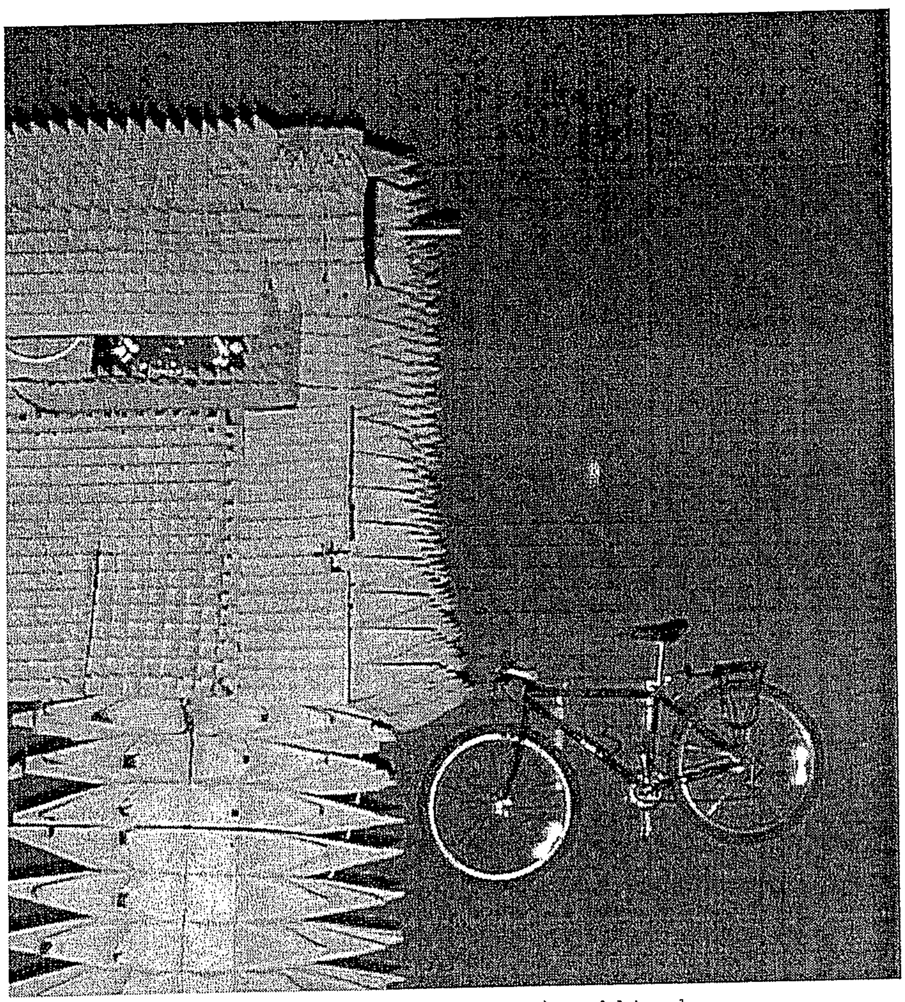

Figure 1: Probe (top center) and bicycle

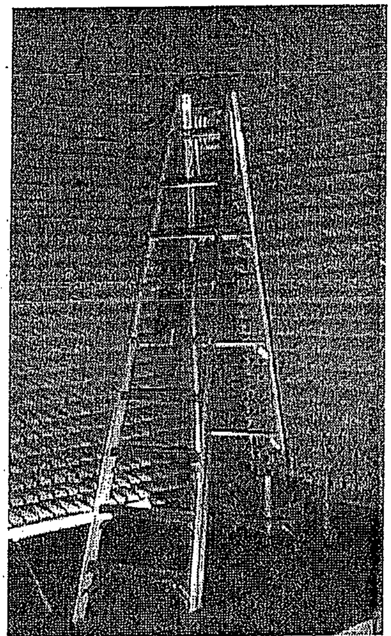

Figure 2: Ladder and plate

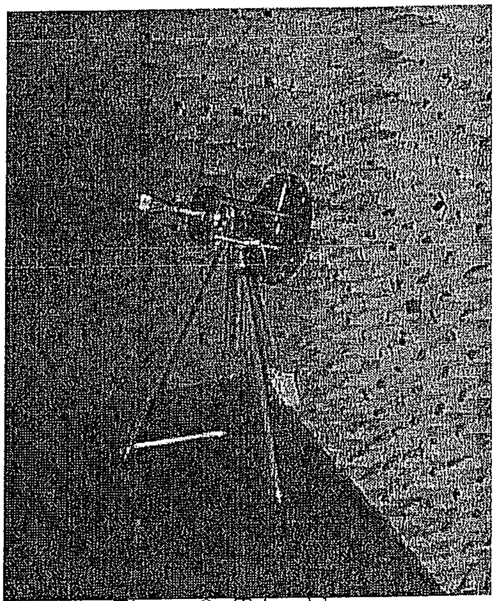

Figure 3: Tripod horn

Images

There is much room for experimentation in the processing of image data for display. We have used the following truncation and scaling procedure:

$$s(\hat{\mathbf{r}}) = \frac{\log\left(\left|\hat{\mathrm{a}}_N(\hat{\mathbf{r}})\right| / s_-\right)}{\log\left(s_+/s_-\right)}. \tag{4}$$

Here, s_+ and s_- determine the dynamic range of the image. Generally $|\hat{\mathrm{a}}_N(\hat{\mathbf{r}})| = |\mathrm{a}_N(\hat{\mathbf{r}})|$, but when $|\mathrm{a}_N(\hat{\mathbf{r}})| > s_+$, we set $|\hat{\mathrm{a}}_N(\hat{\mathbf{r}})| = s_+$, and when $|\mathrm{a}_N(\hat{\mathbf{r}})| < s_-$, we set $|\hat{\mathrm{a}}_N(\hat{\mathbf{r}})| = s_-$. Then $s(\hat{\mathbf{r}})$ is used to produce a bitmap image where $s(\hat{\mathbf{r}}) = 1$ corresponds to maximum intensity and $s(\hat{\mathbf{r}}) = 0$ to black.

In Figures 4 and 5, the tripod horn is the source of radiation. Figure 4 is focused on the bicycle and Figure 5 is focused on the ladder. The bicycle is clearly recognizable along with some structural detail. The ladder, however, is only weakly illuminated. In particular the attached metal plate is not obvious, presumably because the specular reflection is not directed through the measurement sphere. (In Figures 4 and 5, θ varies from $-\pi/2$ to $\pi/2$ vertically and φ varies from π to $-\pi$ horizontally. The lower left corners correspond to $\theta = -\pi/2$, $\varphi = \pi$.)

In an effort to improve the effective dynamic range, measurement 2 was done with a higher gain probe.

Although the emphasis of this presentation is on imaging results, we note that it is possible to determine the best-fit plane wave to the incident field $\mathbf{E}_i(\mathbf{r})$ and the departure of the incident field from the best-fit plane wave. This allows us to characterize the quality of a compact range test zone.

Figure 4: Image focused on bicycle

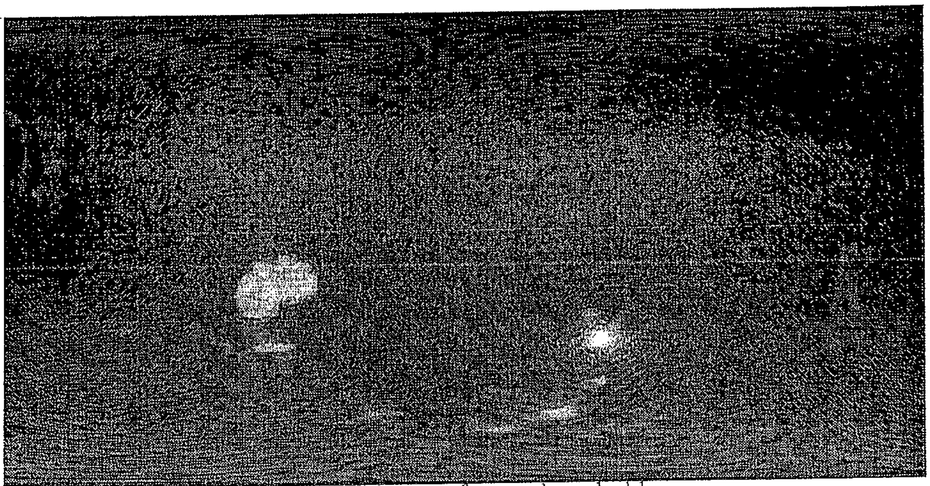

Figure 5: Image focused on ladder

References

[1] J. D. Jackson, *Classical Electrodynamics*, 2nd edition. New York, Wiley, 1975.

[2] R. C. Wittmann, "Spherical near-field scanning: Determining the incident field near a rotatable probe," *1990 IEEE Antennas and Propagation Symposium Digest*, pp. 224-227, May 7-11, 1990.

[3] R. C. Wittmann, and D. N. Black, "Antenna/ RCS range evaluation using a spherical synthetic aperture radar," *Proc. AMTA*, Seattle, pp.406–410, Sept. 30–Oct. 3, 1996.

[4] R. C. Wittmann, and M. H. Francis, "Antenna Range Imaging," *Proc. AMTA*, Philadelphia, pp.234–236, Oct. 16–20, 2000.

[5] R. C. Wittmann, B. K. Alpert, and M. H. Francis, "Near-field antenna measurements using nonideal measurement locations," *IEEE Trans. Antennas Propagat.*, vol. AP-46, pp. 716–722, May 1998.